Title

Scanning laser ophthalmoscope design with adaptive optics

Permalink

https://escholarship.org/uc/item/28k7z4xs

Authors

Laut, Sophie P
Jones, Steven M
Olivier, Scot S
et al.

Publication Date

2005-11-09

DOI

10.1117/12.630975

Peer reviewed

Scanning Laser Ophthalmoscope Design with Adaptive Optics

Sophie P. Laut[*], Steven M. Jones[†], Scot S. Olivier[†], John S. Werner[*]

[*] University of California Davis, Department of Ophthalmology and Vision Science,
4860 Y Street, Sacramento, CA 95817
Phone (916)-734-5839, splaut@ucdavis.edu; Phone (916)-734-6817, jswerner@ucdavis.edu,

[†] Lawrence Livermore National Laboratory, 7000 East Avenue, Livermore, CA 94550
Phone (925)-424-4777, stvnjns@llnl.gov; Phone (925)-423-6483, olivier1@llnl.gov

A design for a high-resolution scanning instrument is presented for *in vivo* imaging of the human eye at the cellular scale. This system combines adaptive optics technology with a scanning laser ophthalmoscope (SLO) to image structures with high lateral (~2 µm) resolution. In this system, the ocular wavefront aberrations that reduce the resolution of conventional SLOs are detected by a Hartmann-Shack wavefront sensor, and compensated with two deformable mirrors in a closed-loop for dynamic correction and feedback control. A laser beam is scanned across the retina and the reflected light is captured by a photodiode, yielding a two-dimensional image of the retina at any depth. The quantity of back-scattered light from the retina is small (0.001% of reflection) and requires the elimination of all parasite reflections. As an *in vivo* measurement, faint cellular reflections must be detected with a low-energy source, a supraluminescent laser diode, and with brief exposures to avoid artifacts from eye movements. The current design attempts to optimize trade-offs between improved wavefront measurement and compensation of the optical aberrations by fractioning the light coming to the wavefront sensor, better sensitivity by increasing the input light energy or the exposure time and the response speed of the system. This instrument design is expected to provide sufficient resolution for visualizing photoreceptors and ganglion cells, and therefore, may be useful in diagnosing and monitoring the progression of retinal pathologies such as glaucoma or aged-related macular degeneration.

Keywords: retinal imaging, Scanning Laser Ophthalmoscope, adaptive optics.

INTRODUCTiON

The invention of the scanning laser ophthalmoscope (SLO) dates from the early 1980's by Webb et al. [1, 2]. The technique is different from that used in classical fundus imaging instruments: parallel rays of light, sent to the pupil of the patient, are focused onto the retina as a point of light. Scanners move the spot systematically across the surface of the retina at a high frequency. From each illumination point, the tissues scatter and back-reflect a very tiny fraction of the incoming beam, which is detected upon return by a sensitive photodetector. After descanning the detected signal received by the sensor and rapid computer processing, a 2-D image of the back-reflection of the scanned surface of the retina is then available in real-time. An optical trombone permits the depth of the scanned area to be varied. A confocal pinhole, conjugate to the point of focus inside the retina, is placed in front of the photodetector to increase the contrast of the image by blocking the back-reflected light outside the focal point plane [3]. The use of a pinhole in front of the photodetector opens the possibility of imaging axial slices of the retina at a resolution close to few hundred microns. Unfortunately, because of diffraction effects resulting from the limited size of the pupil of the eye, and other optical aberrations in the eye, the lateral size of the focused point is limited to approximately 25 µm, affecting the whole lateral resolution of the conventional instrument [4]. To overcome the problem of diffraction effects, the pupil of the patient may be dilated (typically 7 mm by young subjects), however, this is of limited value because of the increasing influence of

the high-order aberrations and the blurring effect that results from it. The common solution consists then in implementing an adaptive optics compensation loop in order to reduce and optimally eliminate the high-order aberrations and, hence, to obtain an almost aberration-free image limited only by the diffraction effects of the pupil. By incorporating adaptive optics (AO), the resolution of the SLO improves to a few microns. The AO system may be incorporated into the classic architecture of a conventional SLO. This requires a wavefront sensor to detect the aberrations, typically a Hartmann-Shack wavefront sensor (HS-WFS), a wavefront corrector (DM) to compensate the aberrations, and a control system with a powerful algorithm for system regulation and optimization implemented with a laboratory computer. The system correction typically occurs at a frequency greater than 20 Hz to correct the temporally-varying aberrations in human eyes [5].

This paper presents the design of an AO SLO. The first section describes the trade-offs in the specification of the different devices typical of a classical SLO. The second part explains the specification of the AO components of the system, and the consequences for the final performance of the aberration compensation. The third section presents the design of a non-aberration-free secondary imaging system: a fundus imager, employed as a view-finder for localizing the imaged area in our AO SLO. We describe the possible choices for the illumination system resulting directly from our light budget.

SLO COMPONENTS

1. AO SLO's specifications

Table 1 shows the principal characteristics of our system and compares them with the specifications of similar systems currently in use [6, 7], as summarized by Table 1. The maximum scanning range of $\pm$ 3 degrees was based upon commercial instrumentation operating at the same speed of signal acquisition. A view-finder, without AO correction, provides a 20 degree fundus image the retina.

	Pablo Artal - Spain	Austin Roorda - UC Berkeley	UC Davis + LLNL
SLO PART			
Light delivery	Laser diode (785 nm)	Laser diode + single-mode fiber	SLD (670 nm) + 820 nm
Optical Power illumination at the eye	100 MicroWatts		100 - 500 MicroWatts
Diameter of incoming beam	2.5 mm		~7 mm
Best focused spot size	~10 Microns (with AO)	2.5 Microns	2.5 Microns
Raster scanning	15 Hz frame rate	16 kHz (resonant scanner)	15 kHz (resonnant scanner)
Scanning range	1 to 10 degrees	1.5-1.4 degrees	+/- 3 degrees at the eye
		Resonant + Galvo Scanner	max. ~6 degrees (Resonant scanner)
			max. ~12 degrees (Galvo scanner)
		525 lines / frame	525 lines / frame
Light detection	PMT	GaAs PMT	PMT
Optical Power coming out of the eye	~10 nW	~30pW	~50 pW
Pinhole diameter	~200 Microns (75 Microns at Retina)	80 Microns	
Depth of focus	~200 Microns	100 Microns axial resolution	
Diameter of exit beam		3.5 mm	
Frame grabbing		30 frames/s	27 frames / s
Image sizes	400x400 pixels	512x512 pixels	512x512 pixels
		Matrox frame grabber	Matrox frame grabber
ADAPTIVE OPTICS PART			
Diameter of the working Pupil	4 mm	7 mm	7 mm
Wavefront sensing		Hartmann-Shack	Hartmann-Shack
AO Controller		Zernike fitting up to the 8th order	PI-controller + Least-Mean-Square Inversion method
Wavefront compensation	37-channel MDM (Okotech)	37-channel DM (Xinetics)	bimorph DM (AOptix) + MEMS (Boston MicroMachines)
			35 actuators + ~100 actuators

Table 1 : *Comparison of the specifications and performance of AO-SLO systems.*

2. Scanners, light delivery and photodetector

The key elements of classical SLO architecture include two scanners (one fast resonant scanner working at 15 kHz and a slower galvanometric scanner working at 27 frames per second), one light source and a photodetector recording the back reflection of the scanned retina. The two scanning mirrors need to be conjugated to the entrance pupil of the system so that the beam is stationary in the pupil of the eye.

The pupil of the eye is assumed to be dilated to 7 mm to obtain a 3 degree field of view of the scanned retina with maximum resolution. The scanning mirrors are positioned as close to the eye as possible so that the light path in the optical system is as static as possible. The light source and the light detector are placed in planes conjugate with the retina. The light source for the scanning part of the system is also used for the wavefront analysis and compensation of the local pupil aberrations of the eye. The light enters and exits through all the components of the set-up; this double-pass technique makes it easier to control and correct the aberrations of the system.

An 820 nm supra-luminescent diode with wide spectral frequencies is used in such a way that the light penetrates the retina to a depth of ~300 μm. A 630 nm light source was chosen for alignment purposes. The light detector is a photomultiplier (PMT) interfaced with a computer to reconstruct an image size of 512x512 pixels.

3. Relay telescopes

Because of back-reflections from lenses, our system is designed with spherical mirrors only. An additional advantage is that this system is insensitive to the choice of wavelengths. The determination of the telescopic relay magnifications depended on the physical sizes of each element. All relay telescopes were arranged in a "4f-like" manner. The transverse magnification ratio for the whole AO SLO is equal to 1.44. The spherical mirrors are off-the-shelf components so that the cost of the system is minimized.

The incident angles of the beam onto the spherical mirrors was simulated with Zemax, limiting and controlling the aberrations of the optical system itself. The relay telescopes that "see" the scan needed to be designed to have low, static, aberrations across the entire scanned field. Hence, static astigmatism and defocus may be removed with a trial lens. The other relays were less critical because their aberrations are static, as long as their final aberration correction doesn't require too much stroke from the wavefront correctors.
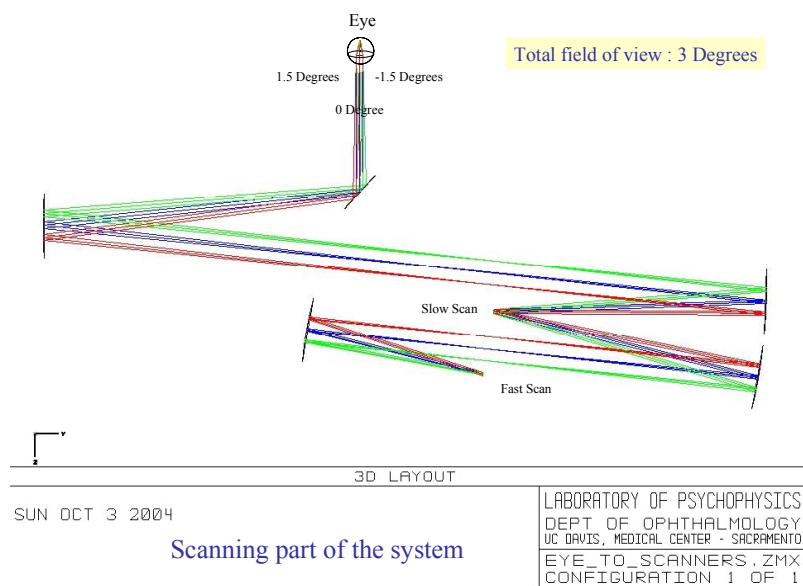
Figure 1: *Zemax simulation for the scanning part of the AO-SLO system.*

Figure 1 shows a Zemax simulation of the $\pm$ 1.5 degree field-angle of the beam in the path between the eye and the two scanners. Figure 2 represents the aberration due to the spherical mirrors obtained for a ray of light exiting the eye after the scanners. Notice that this aberration consists mostly of astigmatism; however, it is important to note that at this point of the set-up, this aberration stays constant through the whole field-of-view of the instrument onto the retina. Hence, as long as this aberration is within a respectable range of values, it is well corrected by cylinder trial lenses.
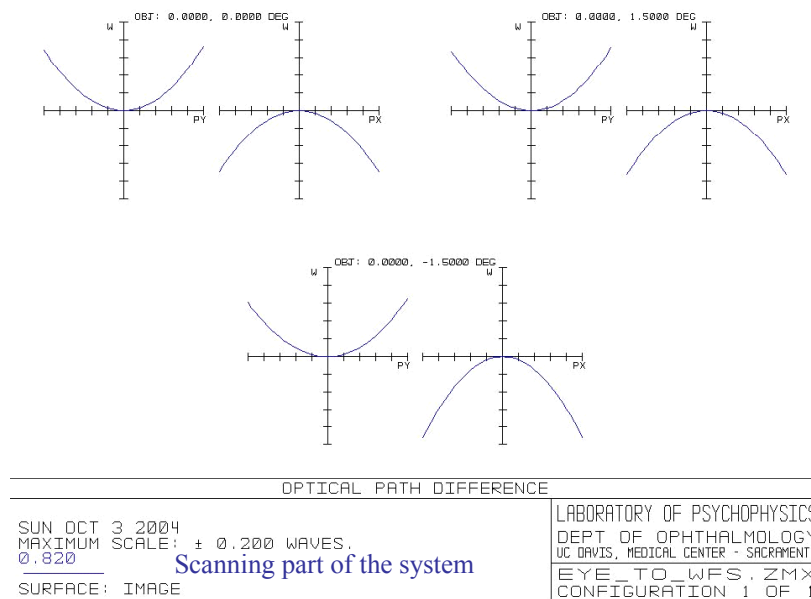
Figure 2: *Optical-Path-Difference displayed respectively at -3 degrees, 0 degree and +3 degrees field-of-view for the scanning part of the system*

4. Optical trombone

An optical trombone is introduced in the system to vary the focusing point of the scanned beam within the depth of the retina. The trombone was placed in a converging-diverging beam. By use of two mirrors mounted on a translation stage, the trombone theoretically generates a maximum axial displacement of 300 µm in the retina for 27 cm optical path difference (~20 cm translation of the trombone), corresponding to a 1 D vergence at the eye and 0.5 D on the bimorph DM (roughly 3 µm stroke on the DM). The trombone was necessarily placed in the path of the WFS; otherwise the WFS would have seen a focus change as the axial scan was performed. The trombone was placed downstream from the scan mirrors so that the aberrations did not change in the relay telescopes that see a scanned field. The location was chosen such that the trombone could generate the maximal vergence change relative to the pathlength.

## 5. Final static aberration of the system

The system is designed to limit the system's aberration to the low orders, defocus and astigmatism, and to make these aberrations conform to values of off-the-shelf trial lenses. These corrective lenses were planned to be set in front of the WFS and PMT. Figure 3 shows the total aberration of the whole system, equaling approximately two waves. Figure 3 (b) shows that the two waves peak-to-valley wavefront aberration of the system corresponds to an astigmatism of 0.25 D, which could easily be corrected by a conventional trial lens.
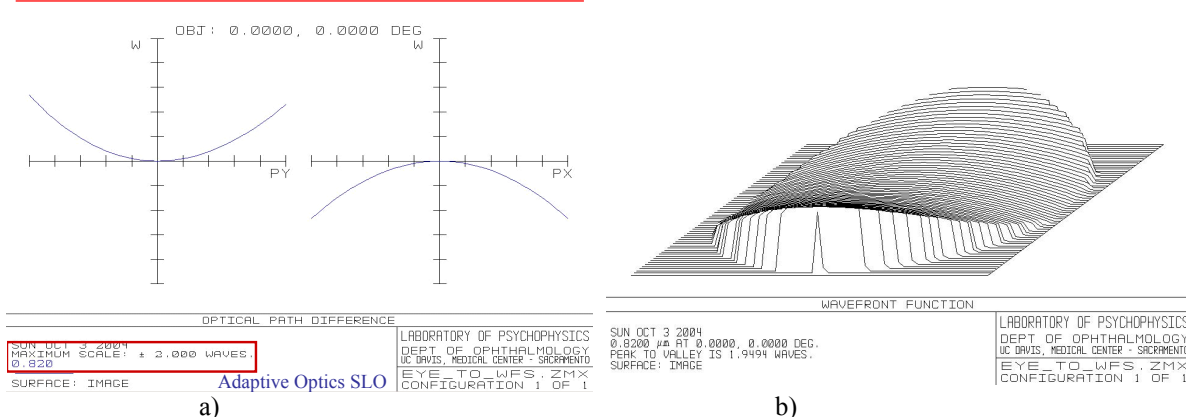
Figure 3: *Final static wavefront aberration of the system, measured at the HS-WFS plane : a) Ray trace curves of the aberration, corresponding mostly to astigmatism; b) Peak-to-valley optical path difference of the corresponding wavefront, estimated to roughly 2 waves (0.25 D cylinder).*

The global SLO system fits on a 1x2 meter optical bench, which was a convenient size for a prototype. This permits easy additional or removal of components in the system compared to a more compact version of the AO-SLO.
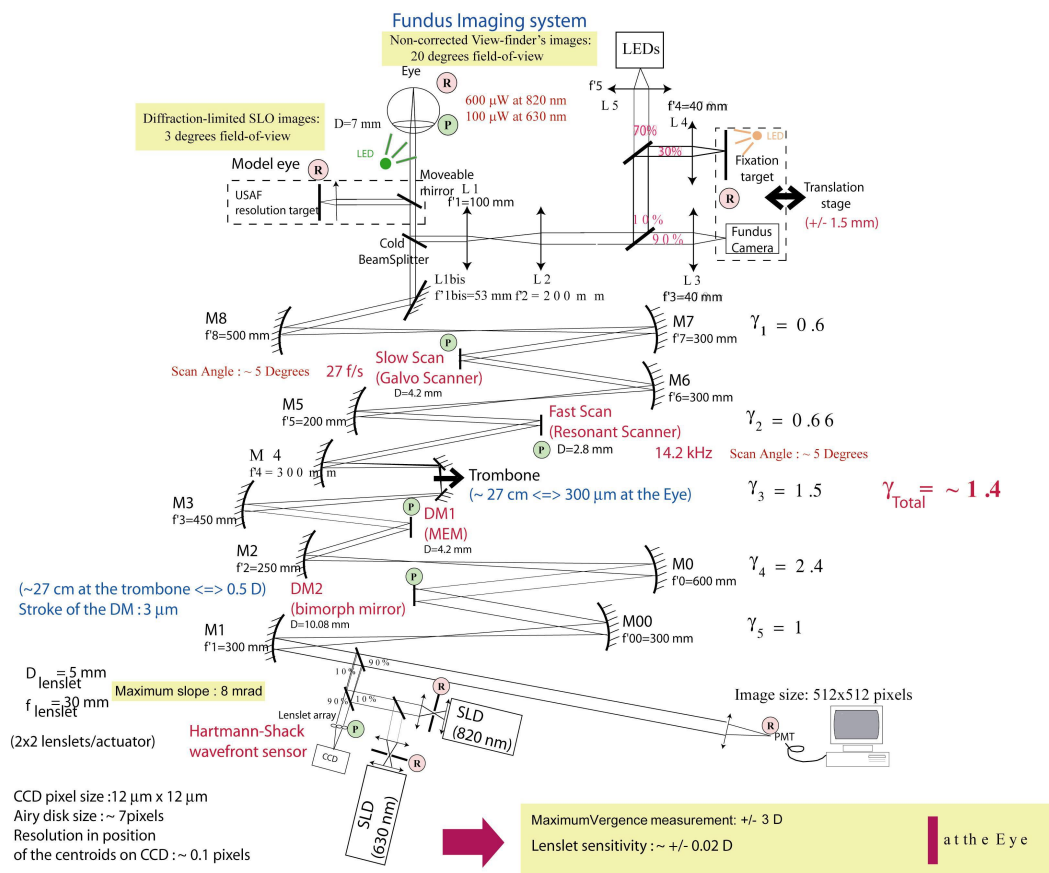
Figure 4: *Schematic of the UC Davis' AO SLO.*

ADAPTIVE OPTICS COMPONENTS

The key parts of the AO system were two DMs and a Hartmann-Shack wavefront sensor. Two DMs were cascaded to provide more stroke to correct the eye aberrations. The bimorph mirror could also be used to correct the patient prescription in the SLO arm of the system. The DM and lenslet array were conjugated to the eye. The maximum incident angle of the beam onto the deformable mirrors was set to 8 degrees.

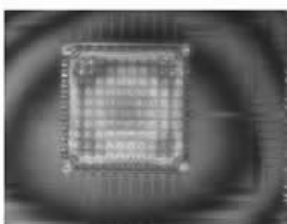## 6. Micro-Electro Mechanical System

The first DM was a microelectrical-mechanical system (MEMS) device from Boston Micromachines. Its active area was 4x4 mm, with 144 actuators (approximately 100 actuators in the pupil area) and a maximum stroke for the wave front of $\pm$ 2 µm. A precise description of its working process, capabilities and characteristics have been described elsewhere [8]. It has been shown that this device is able to provide a factor of four decrease in the root-mean-square (RMS) of the wavefront aberration of a human eye (with defocus corrected by a trial lens) and approximately an 8.5 times improvement in the Strehl Ratio for a 4.6 mm pupil. This stroke is insufficient to correct the aberrations of the eye with defocus and astigmatism included. In our design, this device is used primarily for correction of high-order aberrations.
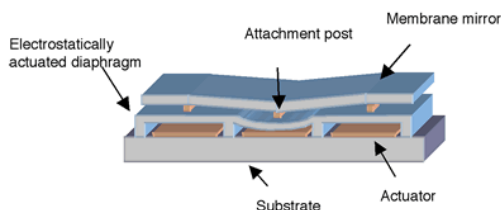
The Boston Micromachines MEMS mirror
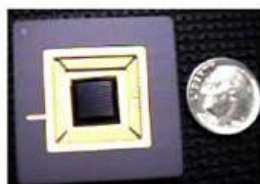
MEMS mirror and a dime   Zygo Interferogram

- Active area : 4 mm x 4 mm
- No of actuators : 100
- Continuous surface
- Stroke (wavefront) : +/- 2 µm
- Response speed : ~3.5 kHz
- Operative voltage : 200 V
- Cost : ~ $25,000

Figure 5: *Cross-section of the MEMS from Boston MicroMachines; specification of the device; picture displaying the size of the MEMS to a dime; Zygo interferogram of the surface of the DM.*

7. AOptix Bimorph Deformable mirror

The second DM is a bimorph type device. Its characterization has been previously studied in both open-loop [9], and closed-loop systems at UC Davis [10].
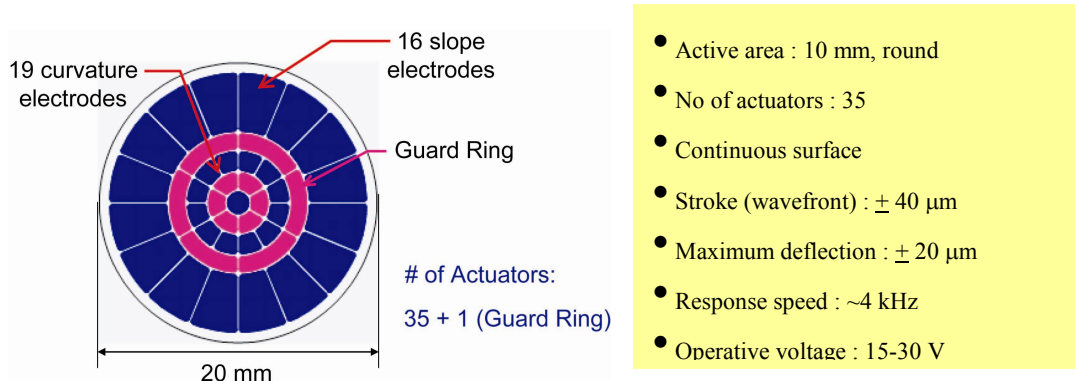
Figure 6: *Ilustration of the bimorph DM and its actuators; specification of the device.*

The active area of this DM is a round membrane of 12 mm with 35 actuators and a maximum stroke for the wavefront of $\pm$ 40 µm corresponding to $\pm$ 3 D (see Figure 6). Because of its large stroke due mostly to the geometry of the actuators and their radial distribution across the surface, this DM was well suited for defocus and astigmatism correction (Figure 7).

The transverse magnification ratio of the system between the entrance pupil of the system and the bimorph was equal to 24.5. Hence, 1D defocus at the patient's eye corresponded to roughly 0.5 D wavefront defocus at the bimorph DM (corresponding to 3 µm of stroke). This value can be compensated by the DM. The mirror was thus able to correct for $\pm$ 3 D at its pupil plane, corresponding to approximately $\pm$ 6 D at the entrance pupil of the system. Such a large compensation capacity for low-order aberrations was particularly attractive in the case of our system: the DM can correct for the prescription of the patient and eliminate the use of trial lenses for this particular purpose while and restricting back-reflections into the system.
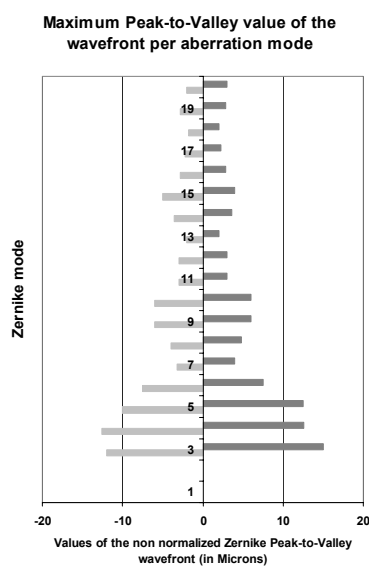
Figure 7: *Maximal peak-to-valley value of the generated wavefront per Zernike mode, for the AOptix deformable mirror.*

8. Hartmann-Shack wavefront sensor

A Hartmann-Shack wavefront sensor is placed in the output conjugate pupil plane. It consists of a lenslet array and a CCD camera in the focal plane of the lenslets. The determination of the lenslet array was based on the trade-off between the number of sampling points on the wavefront surface and the amount of light exiting the eye. Because the measurements were *in vivo*, the energy sent into the eye was limited to about 100 µW in the visible and 600 µW in the near-infrared, requiring a highly sensitive CCD camera with low background noise for the measurement of the back reflection of the retina.

The number of lenslets must be 1-2 times the number of actuators on the MEMS DM to avoid waffle effects resulting in a miscontrol of actuators on the DM. The choice of the last relay telescope in the system just before the wavefront sensor was also important because it set the output beam diameter, and hence the dimension of the lenslets. The lenslet array has a diameter of 5 mm and a focal length of 30 mm for a total beam size of 10 mm at the output of the system; this corresponds to a ratio of 2x2 lenslets per actuator. The maximum slope measurable by the lenslet array was 8 mrad corresponding to a vergence of $\pm$ 3 D at the eye. The CCD pixel size was 12x12 µm, enabling resolution of the position of the centroids onto the CCD to 0.1 pixels. The lenslet sensitivity corresponds to approximately $\pm$ 0.02 D at the eye.

The ratio between the amplitude of the wavefront recorded at the HS-WFS and the amplitude of the wavefront in the entrance pupil of the system was equal to the longitudinal magnification ratio of the system which is approximately 2. Hence, the value in Diopters of the defocus measured at the HS-WFS plane was equal to the value of defocus present in the entrance pupil plane of the system, times 0.47. The maximal slope at the HS-WFS plane, associated with 1 D defocus at the pupil of the eye was $\pm$ 2.5 mRadians. The corresponding peak-to-valley value of the wavefront aberration measured by the HS-WFS plane and associated with 1 D value defocus at the pupil of the eye was equal to 6 µm. The maximal sensitivity of the lenslet array was $\pm$ 1.74 D at the HS-WFS plane, hence $\pm$ 3.7 D at the pupil of the eye ($\pm$ 9 mRadians associated with the maximal slope onto the HS-WFS, and 22.5 µm peak-to-valley value for the wavefront at the HS-WFS). One pixel displacement of the centroids into the CCD plane corresponds to $\pm$ 3 MicroRadians.

DESIGN OF THE FUNDUS IMAGER

The second arm of our AO-SLO design was a fundus imaging system used as a viewfinder with a 20-degree field of view (~6 mm of retina). The major components include an LED (or a set of LEDs) as a light source, a CCD/fundus-pupil camera and a fixation target illuminated by another LED. By switching from the lens L1 to L1bis, the fundus camera may be used to align the pupil of the patient to the entrance pupil of the system (Figure 8).

The fixation target and the fundus camera are on the same translation stage so that the patient focuses the fundus camera onto the retina by adjusting the fixation target. A cold beamsplitter makes it possible to image the fundus simultaneously with SLO measurements. A model eye consisting of a lens and a USAF resolution target is used for calibration of the instrument and may be interchanged with a patient eye by moving a shift-mirror. At the eye, $\pm$ 4 D corresponds to ~3 mm translation of the stage. A translation stage sensitivity of 4 µm roughly corresponds to a sensitivity of 0.04 D at the eye for this system.
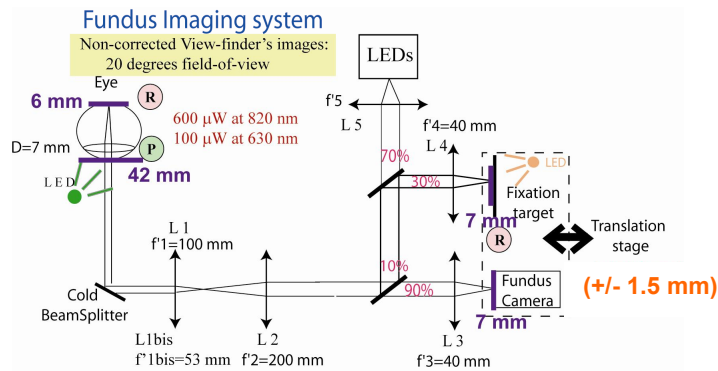
Figure 8: *Non aberration-free fundus camera with a 20 degree field-of-view.*

Figures 9 and 10 show respectively, the Zemax simulation of the Fundus imager, and the quality of the image reconstructions.
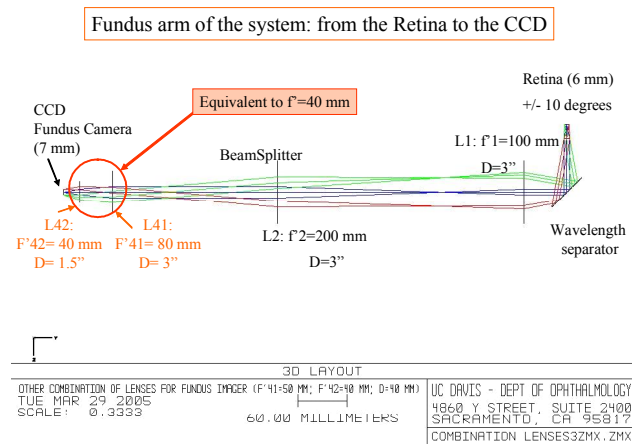

Figure 9: *Zemax simulation of the fundus arm of the system from the retina to the CCD.*
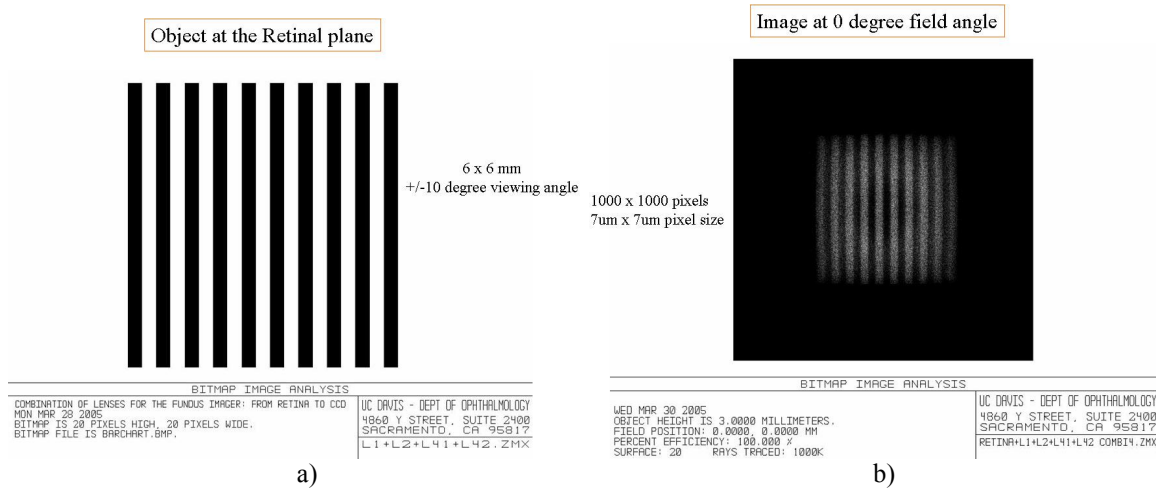

Figure 10: *Zemax simulations of the fundus camera's resolution; a) 6x6 mm object corresponding to a $\pm$ 10 degree field-of-view of the patient's retina. b) corresponding image on axis, with a 1000x1000 pixels and 7x7 μm pixel sized-camera.*

9. Design of the illumination system/light budget

From the Lagrange invariant expression, the following set of LEDs were evaluated as light sources for the fundus imaging arm:

- <u>One LED, 5 mm diameter, Orange (605 nm), 4 cd, viewing angle: 30 degrees</u>

Optical Power at the entrance of the system: 1.55 mW
Optical Power at the Retina: 233 µW

- <u>Set of 24 LEDs, 26 mm diameter, Amber (593 nm), 8.8 cd/each LED, viewing angle: 18 degrees</u>

Optical Power at the entrance of the system: 1.6 mW
Optical Power at the Retina: 247 µW

- <u>Set of 30 LEDs, 33.5 mm diameter, Green (532 nm), 13.2 cd/each LED, viewing angle: 16 degrees</u>

Optical Power at the entrance of the system: 1.67 mW
Optical Power at the Retina: 250 µW

- <u>Set of 30 LEDs, 33.5 mm diameter, Blue (474 nm), 2.85 cd/each LED, viewing angle: 16 degrees</u>

Optical Power at the entrance of the system: 3.4 mW
Optical Power at the Retina: 510 µW

Depending on the size of the light source, the condenser lens at the entrance of the system was estimated to be:
- $F'_5 = 30$ mm $D_5 = 40$ mm   for 5mm-size source
- $F'_5 = 150$ mm $D_5 > 53$ mm   for 26 mm-size source
- $F'_5 = 190$ mm $D_5 = 76.2$ mm   for 33.5 mm-size source

Figures 11 and 12 show the Zemax simulations associated with a single LED-light source and an array of 24-30-LEDs. In each case, the figures show the light path from the source to the retina, and the light path from the source to the eye pupil.

a)   b)
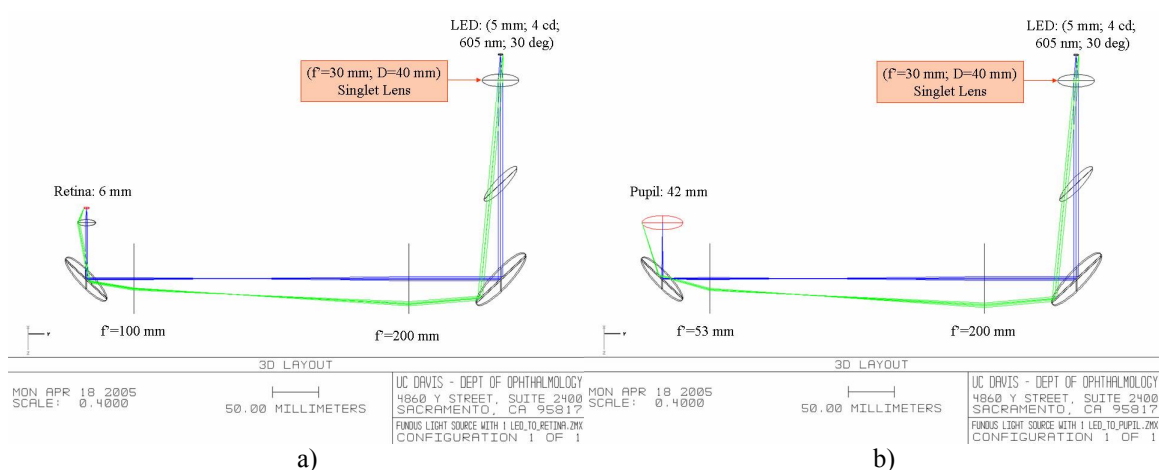
Figure 11: *Simulation of a single LED-light source : a) light path from the fundus illumination system to the retina; b) light path from the fundus illumination system to the pupil of the eye.*
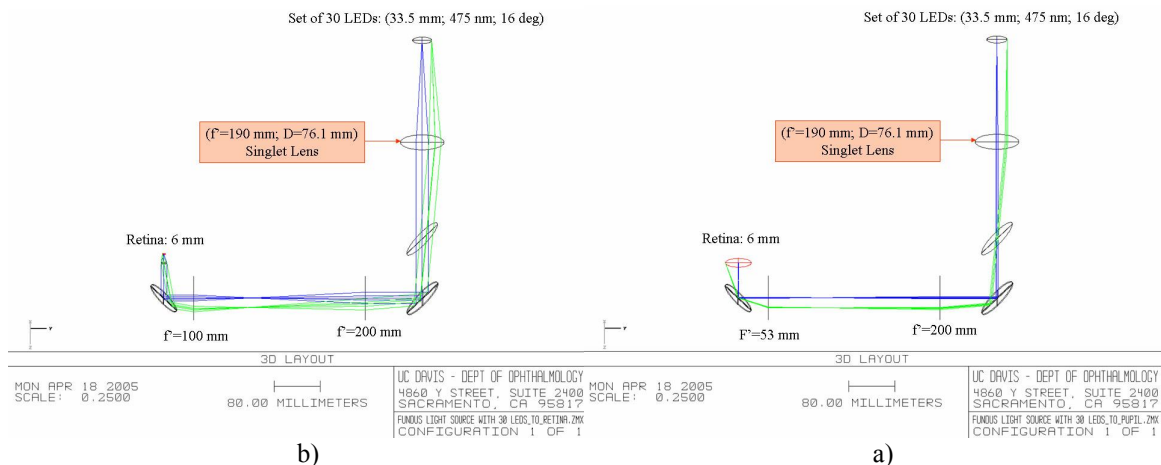
Figure 12: *Simulation of 24 or 30 LEDs as light source : b) light path from the fundus illumination system to the retina; a) light path from the fundus illumination system to the pupil of the eye.*

A light source with dominant wavelength as distinct as possible from the ones used by the SLO part of the system is desireable. However, this suggests a middle wavelength with an intensity that may be uncomfortably bright. Middle wavelengths (530-580 nm) may be used for the target illumination as they match the peak spectral efficiency of human vision.

CONCLUSION

Design of an adaptive optics scanning laser ophthalmoscope is described. The instrument has a lateral resolution equal to a few microns, permitting imaging of the retina at a cellular scale. This system was, to our knowledge, the first attempt in vision science to cascade two deformable mirrors: one bimorph deformable mirror from AOptix was used for the patient prescription correction of defocus and astigmatism; the second deformable mirror was a MEMS from Boston MicroMachines to correct the residual higher-order aberrations after compensation of the majority of the aberrations by the bimorph DM first. We also proposed a design for a view-finder providing a 20 degree field-of-view of the fundus, and defined the associated light budget.

The principal arm of the system was built and associated with the architecture of an optical coherence tomography instrument (OCT)[11]. The first results obtained with the bimorph deformable mirror alone and a spectral-domain OCT arm, confirmed the expected lateral resolution of our design. Further research is currently being conducted to incorporate the MEMS into the system so that aberration compensation will be based on the two DMs working in series.

REFERENCES

1. Webb, R.H. and G.W. Hughes, *Scanning laser ophthalmoscope.* IEEE Transactions on Biomedical Engineering, 1981. **28**: p. 488-492.
2. Webb, R.H., G.W. Hughes, and O. Pomerantzeff, *Flying spot TV ophthalmoscope.* Applied Optics, 1980. **19**: p. 2991-2997.
3. Webb, R.H., G.W. Hughes, and F.C. Delori, *Confocal scanning laser ophthalmoscope.* Applied Optics, 1987. **26**: p. 1492-1499.
4. Liang, J., D. Williams, and D. Miller, *Supernormal vision and high resolution retinal imaging through adaptive optics.* JOSA A, 1997. **14**: p. 2884-2892.
5. Hofer, H., et al., *Improvement in retinal image quality with dynamic correction of the eye's aberrations.* Optics Express, 2001. **8**(11): p. 631-643.
6. Roorda, A., et al., *Adaptive optics scanning laser ophthalmoscopy.* Optics Express, 2002. **10**(9): p. 405-412.
7. Vohnsen, B., I. Iglesias, and P. Artal. *Confocal scanning laser ophthalmoscope with adaptive optical wavefront correction.* in *Three-Dimensional Microscopy: Image Acquisition and Processing X.* 2003: SPIE.
8. Doble, N., et al., *Use of a microelectromechanical mirror for adaptive optics in the human eye.* Optics Letters, 2002. **27**(17): p. 1537-1539.
9. Horsley, D., et al. *Characterization for vision science applications of a bimorph deformable mirror using Phase-Shifting Interferometry.* in *Ophthalmic Technologies XV: Ophthalmic Adaptive Optics, BIOS'2005.* 2005. San Jose (USA): SPIE.
10. Laut, S., et al. *Bimorph deformable mirror: an appropriate wavefront corrector for retinal imaging?* in *Smart Medical and Biomedical Sensor Technology III (SAC118), OpticsEast'2005.* 2005. Boston (USA): SPIE.
11. Zawadski, R., et al., *Adaptive-optics optical coherence tomography for high-resolution and high-speed 3D retinal in vivo imaging.* Optics Express, 2005. **13**(21): p. 8532.